Journal of Catalysis 285 (2012) 196–207

Contents lists available at SciVerse ScienceDirect

Journal of Catalysis

journal homepage: www.elsevier.com/locate/jcat

The coordinatively saturated vanadium MIL-47 as a low leaching heterogeneous catalyst in the oxidation of cyclohexene

Karen Leus [a,1], Matthias Vandichel [b,1], Ying-Ya Liu [a], Ilke Muylaert [a], Jan Musschoot [c], Steven Pyl [d], Henk Vrielinck [c], Freddy Callens [c], Guy B. Marin [d], Christophe Detavernier [c], Paul V. Wiper [e], Yaroslav Z. Khimyak [e], Michel Waroquier [b], Veronique Van Speybroeck [b,*], Pascal Van Der Voort [a,*]

[a] Department of Inorganic and Physical Chemistry, Center for Ordered Materials, Organometallics and Catalysis, Ghent University, Krijgslaan 281-S3, 9000 Ghent, Belgium
[b] Center for Molecular Modeling, Ghent University, Technologiepark 903, 9052 Zwijnaarde, Belgium
[c] Department of Solid State Sciences, Ghent University, Krijgslaan 281-S1, 9000 Ghent, Belgium
[d] Laboratory for Chemical Technology, Ghent University, Krijgslaan 281-S5, 9000 Ghent, Belgium
[e] Department of Chemistry, University of Liverpool, Liverpool L69 3BX, United Kingdom

ARTICLE INFO

Article history:
Received 9 August 2011
Revised 12 September 2011
Accepted 13 September 2011
Available online 19 October 2011

Keywords:
Metal Organic Frameworks
Vanadium
Oxidation catalysis
DFT-D
Epoxidation

ABSTRACT

A Metal Organic Framework, containing coordinatively saturated V^{+IV} sites linked together by terephthalic linkers (V-MIL-47), is evaluated as a catalyst in the epoxidation of cyclohexene. Different solvents and conditions are tested and compared. If the oxidant TBHP is dissolved in water, a significant leaching of V-species into the solution is observed, and also radical pathways are prominently operative leading to the formation of an adduct between the peroxide and cyclohexene. If, however, the oxidant is dissolved in decane, leaching is negligible and the structural integrity of the V-MIL-47 is maintained during successive runs. The selectivity toward the epoxide is very high in these circumstances. Extensive computational modeling is performed to show that several reaction cycles are possible. EPR and NMR measurements confirm that at least two parallel catalytic cycles are co-existing: one with V^{+IV} sites and one with pre-oxidized V^{+V} sites, and this is in complete agreement with the theoretical predictions.

1. Introduction

Metal Organic Frameworks (MOFs) have received an enormous amount of attention over the last decade, as they are considered as the newest generation of porous materials [1,2]. This type of materials is constructed by linking organic ligands with metal ions or metal clusters to form infinite network structures. The porosity, structure, and functionality of the MOF can be tuned by varying the linkers (bridging ligands) and/or the metal centers. MOFs are promising materials for applications in gas adsorption [3,4], separation [5], and catalysis [6–8]. By introducing catalytically active metal-connecting points or functional groups into the highly porous MOF structure, MOFs exhibit clear advantages in heterogeneous catalysis. Moreover, unlike traditional immobilized catalysts [9–11], the active catalytic sites in MOFs are well protected by the coordination bonds that prevent leaching to a higher extent. Although the research in this field is relatively new, MOFs have been studied as catalysts in hydrogenation and oxidation reactions [12–18], enantioselective reactions [19–21], photocatalysis [22], carbonyl cyanosilylation [23–25], hydrodesulfurization [26], and esterification [27].

Catalytic studies on the oxidation of cyclohexene in MOFs have already been published by several groups. For example, the group of Rosseinsky [28] has reported a post-modification procedure of the IRMOF-3 framework with $VO(acac)_2$. They carried out a preliminary catalytic investigation on this modified MOF structure for the oxidation of cyclohexene with *tert*-butylhydroperoxide (TBHP) as the oxidant. Volkmer and co-workers [14] have designed and synthesized a MOF containing unsaturated cobalt sites, namely MFU-1. MFU-1 showed a cyclohexene conversion of 22.5% after 22 h of reaction (theoretically maximum 50% conversion), with *tert*-butyl-2-cyclohexenyl-1-peroxide as the main product (66% selectivity). Garcia et al. recently published a review on the use of MOFs as oxidation catalysts [29]. Recent studies by us [30] have focused on the catalytic performance of a saturated vanadium MOF, namely MIL-47 $V^{IV}O(CO_2–C_6H_4–CO_2)$ [31].

As can be seen from Fig. 1, MIL-47 has a three-dimensional framework, where each V^{+IV} center is coordinated to four oxygen atoms from four carboxylate groups, and to two oxygen atoms on the O–V–O axis, thus forming a saturated octahedral coordination node. The nodes are further connected by sharing the carboxylate linkers and thus grow into a three-dimensional framework. 1D rhombus

* Corresponding authors. Fax: +32 9 264 49 83 (P. Van Der Voort), +32 9 264 65 60 (V. Van Speybroeck).
E-mail addresses: Veronique.VanSpeybroeck@UGent.be (V. Van Speybroeck), Pascal.Vandervoort@ugent.be (P. Van Der Voort).
[1] Both authors contributed equally to this work.

0021-9517/$ - see front matter © 2011 Elsevier Inc. All rights reserved.
doi:10.1016/j.jcat.2011.09.014

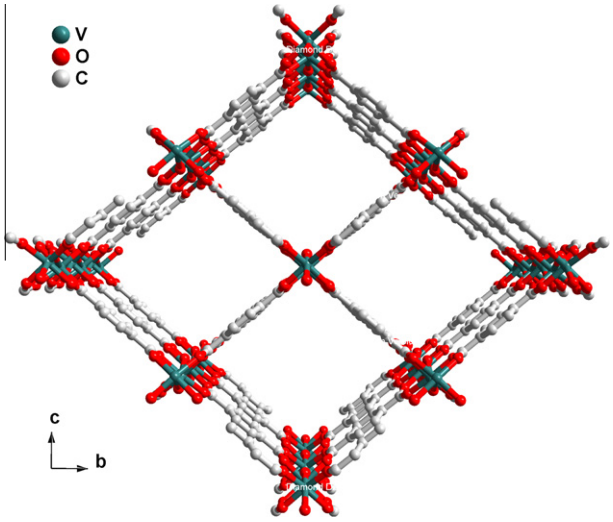

Fig. 1. Perspective view of the structure of MIL-47.

channels are along the *a* axis with sizes of about 10.5 × 11.0 Å (Van der Waals radii excluded) for the channel windows. The structure shows good thermal stability (stable up to 350 °C in air).

Recently, we published the first catalytic evaluation of V-MIL-47 in the liquid phase oxidation of cyclohexene, using TBHP in water as the oxidant and chloroform as the solvent [30]. In general, the liquid phase oxidation of cyclohexene can produce one or more of following products as shown in Scheme 1.

In this paper, we have extended our earlier work to a more in-depth mechanistic study. We examine the catalytic performance of MIL-47 in water and water-free media. In each medium, two catalyst loadings will be considered: 0.11 mmol and 0.42 mmol V-centers in the total reaction mixture. The catalytic activity of the MIL-47 is compared to the homogeneous catalyst $VO(acac)_2$. In order to fully unravel possible reaction mechanisms, which are operative in the MIL-47, an extensive ab initio computational study has been conducted. The nature of the active site is investigated by studying a variety of possible reaction cycles that might occur in the cyclohexene oxidation. Some active sites start from vanadium in oxidation state (+IV) where others produce first vanadium in oxidation state (+V). EPR and NMR measurements were also performed to determine the presence and activity of vanadium in both oxidation states.

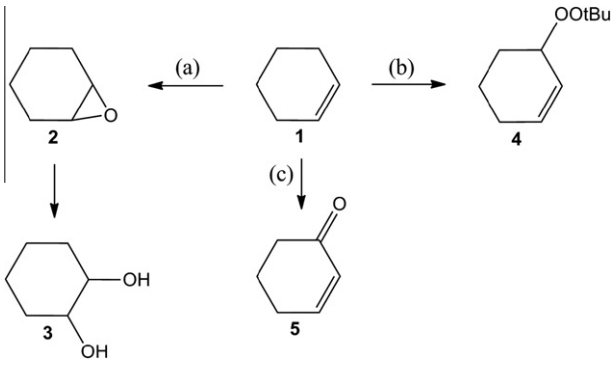

Scheme 1. Oxidation of cyclohexene **1** toward the main reaction products: (a) epoxidation to cyclohexene oxide **2** and consecutive ring opening to cyclohexane-1,2-diol **3**, (b) radical pathway to *tert*-butyl-2-cyclohexenyl-1-peroxide **4** and (c) allylic oxidation to 2-cyclohexene-1-one **5**.

2. Experimental: materials and methods

2.1. General procedures

All chemicals for the synthesis of MIL-47 and the catalytic tests were purchased from Sigma Aldrich (unless otherwise noted) and used without further purification. An ultra-fast GC equipped with a flame ionization detector (FID) and a 5% diphenyl/95% polydimethylsiloxane column with 10 m length and 0.10 mm internal diameter was used to follow the conversions of the products during the catalytic tests. Helium was used as carrier gas, and the flow rate was programmed as 0.8 mL/min. The reaction products were identified with a TRACE GC × GC (Thermo, Interscience), coupled to a TEMPUS TOF-MS detector (Thermo, Interscience). The first column consists of a dimethyl polysiloxane package and has a length of 50 m, with an internal diameter of 0.25 mm, whereas the second column has a length of 2 m with an internal diameter of 0.15 mm. The package of the latter is a 50% phenyl polysilphenylene-siloxane. Helium was used as carrier gas with a constant flow (1.8 mL/min).

X-ray fluorescence (XRF) measurements were performed with an ARTAX (Bruker) Peltier cooled silicon drift detector, using a Mo X-ray source. The detector was placed above the surface of the solution. Spectra were accumulated during 200 s. The system was calibrated by measuring the XRF spectra of different aqueous-based solutions of $VO(acac)_2$ and $Co(NO_3)_2{\cdot}6H_2O$ with known V/Co ratios. Nitrogen adsorption experiments were carried out at −196 °C using a Belsorp-mini II gas analyzer. Prior to analysis, the samples were dried overnight under vacuum at 120 °C to remove adsorbed water. X-ray powder diffraction (XRPD) patterns were collected on a ARL X'TRA X-ray diffractometer with Cu Ka radiation of 0.15418 nm wavelength and a solid-state detector. Electron paramagnetic resonance (EPR) spectra of dry powders were recorded at room temperature with a Bruker ESP300E X-band (9.77 GHz) spectrometer, equipped with a HP5350B frequency counter and a ER035 M gaussmeter. Standard NMR sample tubes (4 mm inner diameter) were filled to a height of approximately 5 mm, and for comparison of intensities, the spectra were divided by the powder mass. For all spectra, the magnetic field was modulated at 100 kHz with an amplitude of 0.2 mT, and the microwave power was set to 2 mW, avoiding saturation.

2.2. Synthesis of MIL-47

MIL-47 was synthesized according to a synthesis route described in literature [31]. Typically, 1.37 g VCl_3 and 0.36 g terephthalic acid were mixed together with 15.7 mL of deionised H_2O. The resulting mixture was transferred into a Teflon-lined stainless autoclave for 4 days at 200 °C. The as-synthesized MIL-47 was filtered, washed with acetone, and calcined for 21 h 30 min at 300 °C to remove free terephthalic acid from the pores. Typical synthesis yield is approximately 15%.

2.3. General procedure for the cyclohexene oxidation

During a typical catalytic test, a 100-mL round-bottom flask was charged with 30 mL of chloroform (anhydrous) used as solvent, 5 mL of cyclohexene, and 6.2 mL of 1,2,4-trichlorobenzene (used as internal standard for the GC analysis). The oxidants used in this paper were *tert*-butylhydroperoxide (TBHP) in water (70%) and TBHP 5.5 M in decane. The molar ratio cyclohexene/oxidant was 1/2. All the catalytic tests were performed at a temperature of 50 °C and with an Ar-containing balloon on top of the condenser. Blank reactions at this temperature showed no catalytic conversion of cyclohexene.

The reaction mixture was stirred under an inert argon atmosphere until a plateau was reached in the cyclohexene conversion. Aliquots were gradually taken out of the mixture, diluted with 500 μl ethylacetate, and subsequently analyzed by GC-FID and GC × GC TOF-MS. After a catalytic run, the catalyst was recovered by filtration on a combined nylon-membrane filter, washed with acetone, and vacuum dried overnight. The filtrate was analyzed by XRF to determine the leached vanadium.

3. Experimental results

3.1. Characterization

In this paper, we will compare the catalytic performance of MIL-47 in water and water-free media. A thorough study of the catalytic performance of MIL-47 is presented, together with a spectroscopic study and a computational model.

3.1.1. Characterization of the catalyst

The MIL-47 had an average Langmuir surface area of 1225 m^2/g and a pore volume of 0.38 ml/g. Only batches of MIL-47 that diverted less than 5% from these values were used in this work. The value of 1225 m^2/g is consistent with literature [31].

The XRPD pattern of the synthesized MIL-47 is presented in Fig. 2 and compared to the XRPD pattern, generated from the original CIF-file [31]. The experimental XRPD pattern of MIL-47 matches perfectly with the simulated pattern, confirming the phase purity of the synthesized MIL-47. Some differences in reflection intensities between the simulated and experimental pattern are due to the variation in crystal orientation of the micro crystals.

3.1.2. The catalytic performance of MIL-47 in the oxidation of cyclohexene

In Fig. 3, the catalytic performance of MIL-47 is shown using respectively TBHP/water (left) and TBHP/decane (right) as oxidant. In this figure, two catalyst loadings (0.11 mmol and 0.42 mmol of V-centers) are considered. The reader should pay attention to the differences in the timescale of the *x*-axes, as all experiments were performed until a linear plateau in the conversion was reached or until a maximum time of 82 h.

Several general trends can be deducted from Fig. 3. (1) Convergence regimes for cyclohexene conversion are reached in all cases, provided sufficient large reaction time is taken into account. (2) The conversion tends toward 80% at the end of the reaction. The lower conversion in Fig. 3c is probably due to a too short reaction time. (3) In the initial stages, the cyclohexene conversion is almost linear in all cases. There are, however, differences in the slope of these linear sections: the 0.42 mmol V catalytic systems start clearly the fastest (approximately 20% conversion per hour for TBHP in water and 7% conversion per hour of TBHP in decane) whereas the 0.11 mmol V systems start much slower (~4% conversion per hour for the TBHP in water and even slower for the TBHP in decane). (4) In the systems that use TBHP in water, the cyclohexene oxide attains a maximum, after which the concentration gradually returns to zero. This is partly due to the transformation of the epoxide **2** into the diol **3** resulting from the reaction with water and terephthalic acid (as shown in Scheme 1). (5) The byproduct **4**, formed via radicalar pathways, grows systematically and exceeds the concentration of the epoxide after sufficient long reaction times. The crossing of those two yields occurs at relative short reaction times for the TBHP in water systems and is heavily delayed by using the TBHP in decane. This is due to the particular role of water in the reaction medium in stabilizing the radical intermediates (see computational discussion, Section 3.2). (6) The formation of the ketone **5** is marginal in all cases. (7) During the first 7 h of reaction, the selectivity toward the cyclohexene oxide is almost 100% in the 0.11 mmol V-sites with TBHP in water system. After that, the product distribution changes. The cyclohexene oxide reaches a maximum of 38% after 25 h of reaction. After that, the cyclohexane-1,2-diol **3** starts to be produced, and the *tert*-butyl-2-cyclohexenyl-1-peroxide **4** becomes dominant (see Table 1).

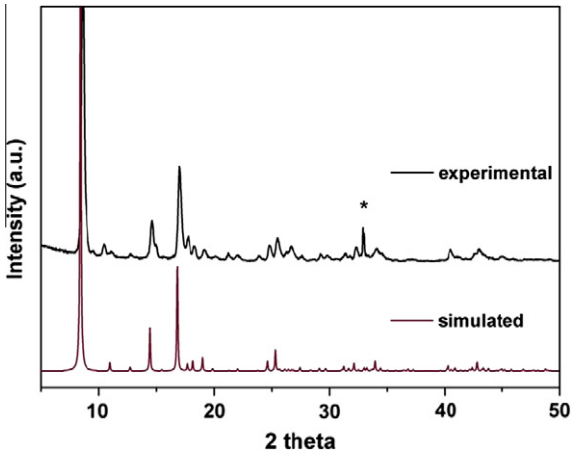

Fig. 2. XRPD patterns of MIL-47 (experimental and simulated [31]) (* is due to the background of the sample holder at an angle of 32.9°).

The faster kinetics observed in Fig. 3c compared to Fig. 3a are mainly due to the higher V-loading. But in both cases, also a significant amount of leached V is observed. Our earlier work [30] showed that after 1 h of catalysis, 12.8% of the V is leached out of the structure with 0.11 mmol of V-sites.

In order to reduce this leaching, the catalytic performance of MIL-47 in the oxidation of cyclohexene was analyzed with TBHP/decane as oxidant (see Fig. 3b and d). When the catalytic performance of MIL-47 in the water-based media is compared to the water-free media, then it is clear that the cyclohexene conversion is approximately 30% after 7 h of reaction with TBHP/decane as oxidant, while the total cyclohexene conversion in the water dissolved TBHP system is much higher in the initial stage (55% after 7 h of reaction). Furthermore, it is interesting to note that, as the conversion is lower, the selectivity toward the cyclohexene oxide is remarkably higher. In Table 1, the selectivity toward the cyclohexene oxide with TBHP/water and TBHP/decane as oxidant is shown for each V-loading, together with the TON and TOF of MIL-47 and $VO(acac)_2$. This Table 1 shows that the selectivity in TBHP/decane is significantly higher compared to the water-based equivalent.

The presence of water during the catalytic test clearly affects both the rate of the epoxidation reaction and the stabilization of radical species toward the formation of the adduct **4.** More details about the reaction mechanisms for both systems are given in the computational sections (vide infra). The former effect might be partly due to vanadium leaching. Only a negligible amount (<3%) of vanadium was leached out of the structure when TBHP/decane was used as oxidant after 7 h of reaction, whereas with TBHP/water, after the same time, a V-leaching of almost 50% was observed.

3.1.3. Catalytic performance of $VO(acac)_2$ in the oxidation of cyclohexene

Next, the catalytic performance of MIL-47 in TBHP/water and TBHP/decane as oxidant was compared with the homogeneous catalyst $VO(acac)_2$ in identical conditions and V-loadings. In Fig. 4, the cyclohexene conversion and yield of cyclohexene oxide **2**, cyclohexane-1,2-diol **3,** and the *tert*-butyl-2-cyclohexenyl-1-peroxide

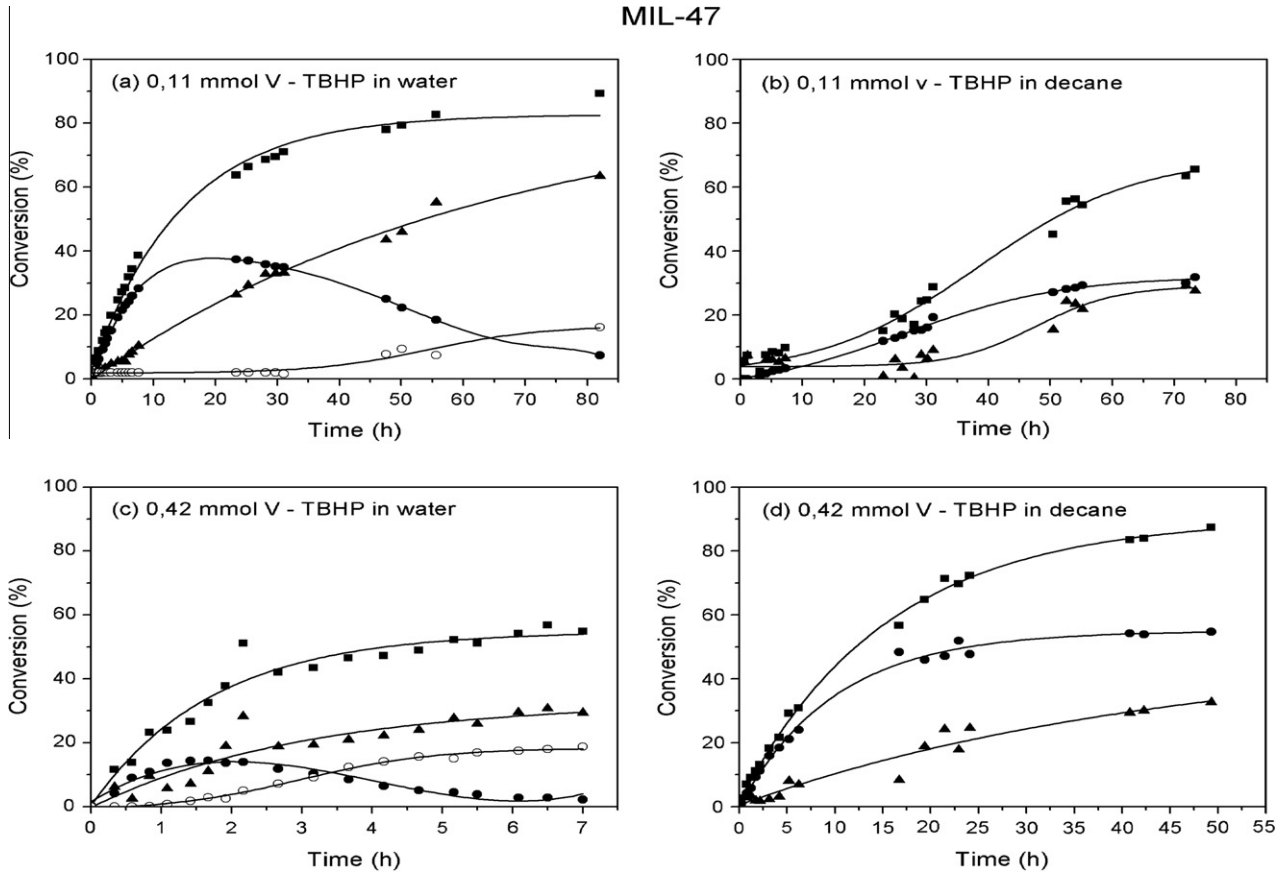

Fig. 3. Cyclohexene (**1**) conversion (■) and the yield of cyclohexene oxide (**2**) (●), *tert*-butyl-2-cyclohexenyl-1-peroxide (**4**) (▲) and cyclohexane-1,2-diol (**3**) (○) for MIL-47 in TBHP/water (Left) with 0.11 mmol V-sites (a) and 0.42 mmol V-sites (c); and for MIL-47 in TBHP/decane (Right) with 0.11 mmol V-sites (b) and 0.42 mmol V-sites (d). No cyclohexane-1,2-diol (○) is formed when TBHP in decane is used. The production of 2-cyclohexene-1-one is in all cases less than 5%, for the clarity of the figure this is not shown.

Table 1
Selectivity toward the cyclohexene oxide with TBHP/water and TBHP/decane as oxidant for each V-loading and the TON and TOF of MIL-47 and $VO(acac)_2$.

V-loading (mmol)	Oxidant	Catalyst	TON[a]	TOF (h^{-1})[b]	Selectivity[c]
0.11	TBHP/water	MIL-47	150	30	70
0.42	TBHP/water	MIL-47	67	29	43
0.11	TBHP/decane	MIL-47	42	37	63
0.42	TBHP/decane	MIL-47	28	8	83
0.11	TBHP/water	$VO(acac)_2$	169	44	70
0.42	TBHP/water	$VO(acac)_2$	62	57	25
0.11	TBHP/decane	$VO(acac)_2$	112	35	87
0.42	TBHP/decane	$VO(acac)_2$	74	48	78

[a] TON was calculated after 7 h.
[b] TOF was calculated after 30 min.
[c] The selectivity toward the cyclohexene oxide calculated at 40% cyclohexene conversion.

4 is shown for the $VO(acac)_2$ catalyst respectively in the water and water-free medium for total V-loadings of 0.11 and 0.42 mmol. The reader is again reminded that the *x*-axes have different timescales.

The homogeneous catalyst shows a similar behavior as MIL-47 in the water-based oxidant. Firstly, the cyclohexene conversions reach a plateau after approximately the same time (80% after 70 h for 0.11 mmol and 55% after 7 h of catalysis for 0.42 mmol V-sites). Secondly, for both V-loadings, the cyclohexene oxide **2** attains a maximum after 20 h for the 0.11 mmol V and 2 h for the 0.42 mmol V when the cyclohexane-1,2-diol **3** starts to be produced and the *tert*-butyl-2-cyclohexenyl-1-peroxide **4** becomes the main product. However, comparison of the homogeneous catalyst with the MIL-47 for TBHP/decane as oxidant clearly shows some differences. For the $VO(acac)_2$, the cyclohexene conversion is much faster compared to the MIL-47. After 7 h of reaction, a cyclohexene conversion of 65% is observed for the 0.42 mmol V-sites compared to 30% for the microporous MOF. Likewise, with the lower V content, it can be seen that the cyclohexene conversion is much slower compared to the $VO(acac)_2$ catalyst. Nevertheless, the selectivity of both catalysts toward cyclohexene oxide is more or less the same as can be seen from Table 1.

3.1.4. Stability and regenerability of the catalyst

The crystalline structure of the MOF was examined by X-ray diffraction to verify the stability of the MOF after a catalytic run. In Fig. 5, the XRPD pattern of MIL-47 is shown before and after a

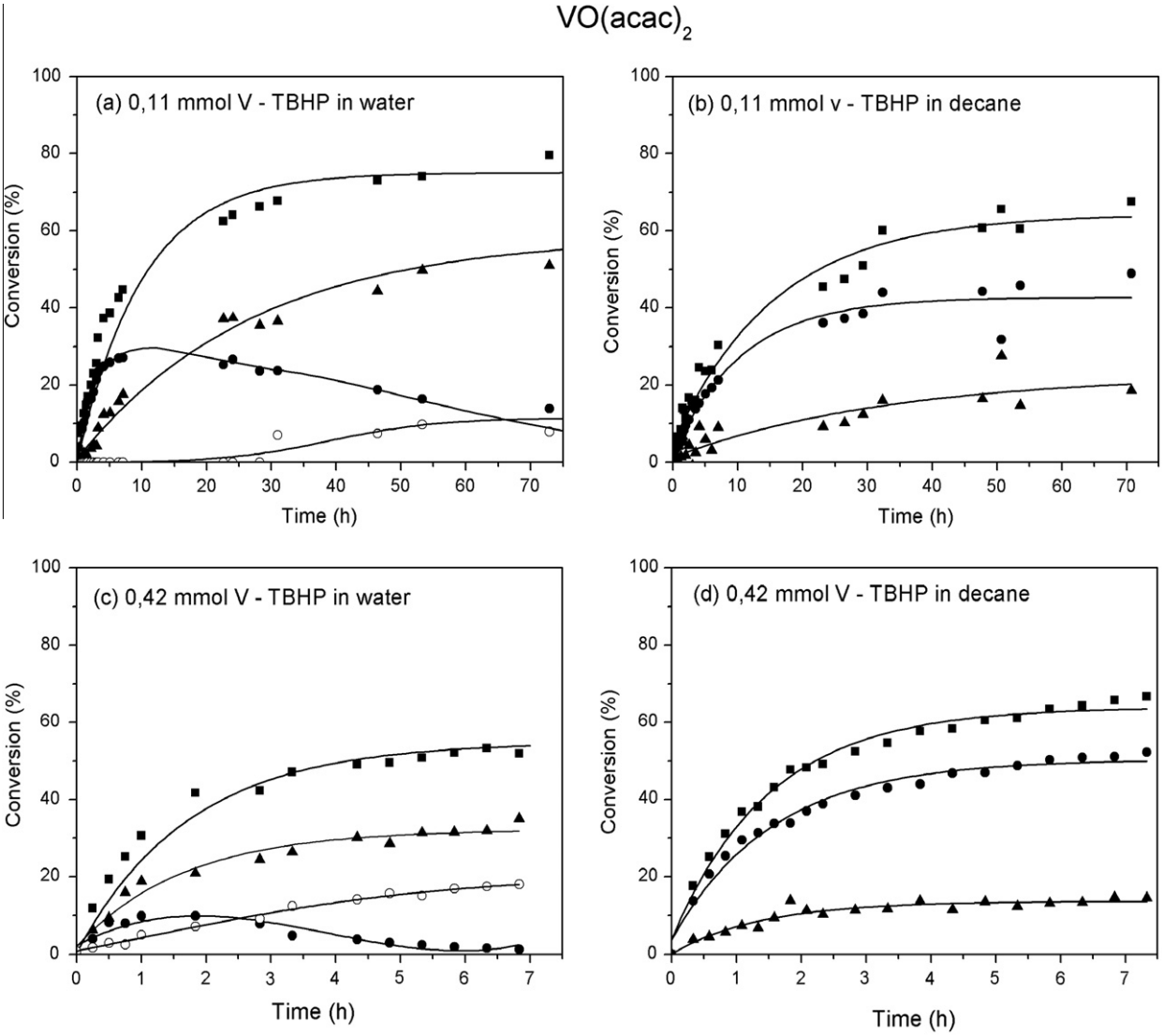

Fig. 4. Cyclohexene (**1**) conversion (■) and the yield of cyclohexene oxide (**2**) (●), *tert*-butyl-2-cyclohexenyl-1-peroxide (**4**) (▲) and cyclohexane-1,2-diol (**3**) (○) for $VO(acac)_2$ in TBHP/water (left) with 0.11 mmol V-sites (a) and 0.42 mmol V-sites (c); and for $VO(acac)_2$ in TBHP/decane (right) with 0.11 mmol V-sites (b) and 0.42 mmol V-sites (d). No cyclohexane-1,2-diol (○) is formed when TBHP/decane is used. The production of 2-cyclohexene-1-one is in all cases less than 5%, for the clarity of the figure this is not shown.

catalytic run, using TBHP/water or TBHP/decane as oxidant at a temperature of 50 °C. Furthermore, the XRPD pattern of the organic linker in MIL-47 (terephthalic acid or BDC, benzene dicarboxylic acid) is shown. As can be seen from this figure, the XRPD pattern of the MIL-47 after a first catalytic run with TBHP in water as oxidant (Fig. 5c) changes significantly compared to the original XRPD pattern (Fig. 5a). Especially, some new diffraction peaks, which can be assigned to the BDC linkers, appear after a first catalytic run. This observation indicates that the structure partially decomposes in the TBHP/water system. This also explains the significant V-leaching that has been observed. Subsequently, MIL-47 was regenerated by a treatment in a tubular furnace under a nitrogen flow at 150 °C for 4 h to remove the organic compounds inside the pores. After this extra step, the structure of MIL-47 was regained as shown in Fig. 5d.

Comparison of the XRPD pattern of MIL-47 before and after a catalytic run, using TBHP in decane (Fig. 5a and b) as oxidant, however, clearly demonstrates that in a water-free medium, the structural integrity of the MOF is entirely preserved. No peaks of free BDC can be observed, and no additional treatment is required to remove these free linkers.

To test the regenerability of the catalyst, four consecutive catalytic runs have been performed in TBHP/decane as oxidant. During each catalytic cycle, the cyclohexene conversion was monitored during at least 6 h. The XRPD patterns of the original MIL-47 and after each run are shown in Fig. 6. As can be seen from this figure, MIL-47 preserves its crystalline structure during these additional runs. The lower signal to noise ratio in run IV is due to the tiny amount of sample that was left for analysis.

In Table 2, the TON and TOF values are shown for MIL-47 in the four consecutive runs. Furthermore, the percentage of leached V in the filtrate is given after each catalytic test. Only in the first cycle, a negligible amount of leached V was observed (<3%), whereas in the following cycles, no leaching was detected. The TON and TOF drop after the first run but remain relatively constant during the next additional cycles. This observation can be explained by the fact that after each run, still some organic compounds of the previous catalytic test clog the pores. This was supported by nitrogen adsorption measurements that showed that the surface area of MIL-47 after a first run dropped from 1225 m^2/g to approximately 500 m^2/g; this will surely lead to a decrease of the reaction rate in the additional runs. We have shown previously [30] that even in

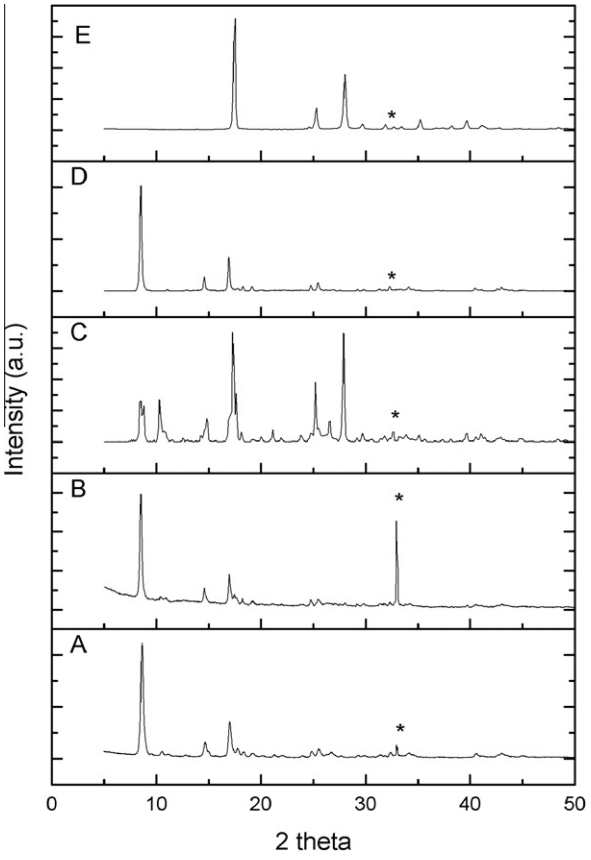

Fig. 5. XRPD pattern of (a) MIL-47, (b) MIL-47 after catalysis with TBHP in decane as oxidant, (c) MIL-47 after catalysis with TBHP in water as oxidant, (d) MIL-47 after regeneration and (e) terephthalic acid (* is due to the background of the sample holder at an angle of 32.9°).

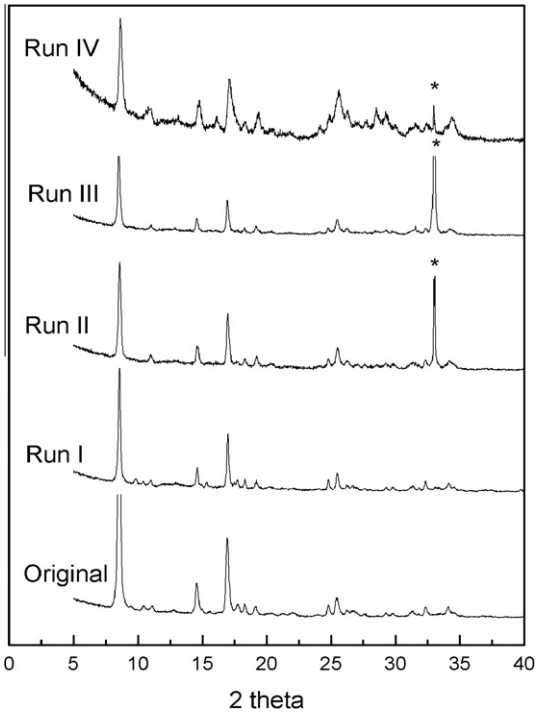

Fig. 6. XRPD pattern of the original MIL-47 before catalysis and the XRPD pattern of MIL-47 after the first, second, third and fourth catalytic run (* is due to the background of the sample holder at an angle of 32.9°).

Table 2
TOF, TON and the percentage of leached V for the consecutive catalytic runs with TBHP/decane as oxidant.

	TON[a]	TOF[b] (h^{-1})	Leaching (%)
Run I	23	7.8	<3
Run II	14	4.8	0
Run III	15.3	2.9	0
Run IV	12.7	3	0

[a] TOF was calculated after 38 min;
[b] TON was calculated after 6 h.

conditions of severe leaching (TBHP in water), still these leached out species are relatively inert for the epoxidation mechanism as the building of epoxide stops immediately after the hot filtration of the catalysts; whereas the radical formation of the adduct **4** continues.

3.1.5. EPR and NMR results

In Fig. 7, the results of room temperature EPR measurements on dry powders of MIL-47 are shown as a function of catalytic reaction time for MIL-47 in TBHP/decane. The inset displays the EPR spectra of the MIL-47 powder and the ML-47 powder after 3 h of catalytic performance. Both spectra appear as broad lines and can be well-fitted by single Lorentzians. The position, which is practically the same in the two spectra, is compatible with a signal assignation to V^{+IV} ($g = 1.96$) [32]. The absence of ^{51}V hyperfine structure is attributed to spin–spin interactions between the close-by V^{+IV} ions in the MIL-47 structure. The width of the spectra, however, is a point of significant difference between the spectra, which will be further addressed in a future investigation.

In the present study, we are mainly interested in the evolution of the total spectral intensity. This was evaluated by double integration of the field-modulated spectra. In order to avoid possible influences of broad background signals, the total intensities were also calculated from the area of the best-fit Lorentzian to the singly integrated spectra. Intensities were normalized to that of the calcined MIL-47 powder. As seen in Fig. 7, the two methods lead essentially to the same conclusions. Within the investigated range of catalytic reaction times, the spectra experience an intensity drop

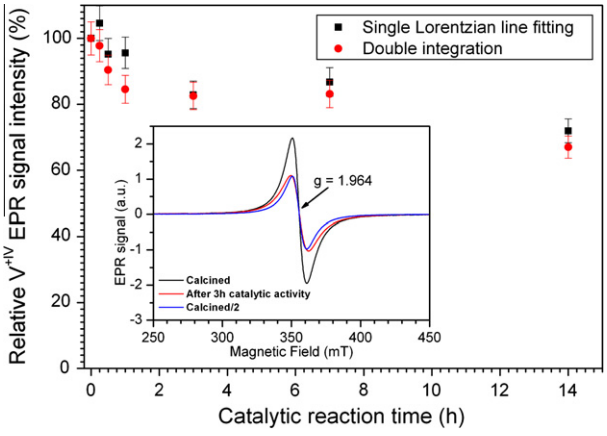

Fig. 7. Catalytic reaction time evolution of the intensity of the EPR spectrum for the MIL-47 in TBHP/decane system. EPR spectra were recorded on dry powders and intensities were evaluated by single Lorentzian fitting to the singly integrated spectra and by double integration. All intensities were normalized to that of the calcined MIL-47. Inset-EPR spectra for calcined MIL-47 (black) and after 3 h of catalytic reaction in the MIL-47/TBHP/decane system (red). For better comparison of the line widths of the EPR spectra, the spectrum of calcined MIL-47 divided by 2 in intensity is shown in blue. (For interpretation of the references to color in this figure legend, the reader is referred to the web version of this article.)

by 20–30%, suggesting that approximately this percentage of the V^{+IV} centers observable with EPR is oxidized to V^{+V}. The major part of the intensity decrease is observed in the first few hours (1–3 h). In the later stages, the EPR intensity seems to stabilize or at least to change far more slowly.

The structural changes around vanadium sites upon calcination of the initial framework are confirmed by ^{51}V solid-state NMR. Due to the paramagnetism of V in the calcined material, a very broad featureless spectrum was recorded. After catalysis, clear presence of V^{+V} in the species is detected and the spectrum profile is reminiscent of that reported for other materials containing V^{+V} species. The spectral profile is consistent with reported complexes containing V^{+V} species [33]. The changes in the environment of vanadium centers after catalysis are reflected in the ^{1}H–13C CP/MAS spectra as much broader peaks are observed for the calcined solids (spectra are shown in the ESI).

3.2. Discussion: theoretical results on reactive pathways for epoxidation

This computational section aims at: (i) defining the active sites for catalysis, (ii) introducing a finite cluster representing the active site within the MIL-47, (iii) proposing plausible reaction pathways for the epoxidation of cyclohexene, and (iv) elucidating the role of the solvent (water versus decane) on the product selectivity in the cyclohexene conversion, as observed in experiment.

3.2.1. Selection of the cluster model

In an undamaged saturated MIL-47 framework, the coordination sphere around the metal ion is completely blocked by the organic linkers, leaving no free positions available for substrate chemisorptions. In our earlier theoretical modeling work on the homogeneous $VO(acac)_2$ catalyst, we found that first vacant coordination sites should be created to activate the catalyst [30]. This is in accordance with earlier literature data [34]. For the MIL-47, free coordination positions should also be created by ligand removal or by folding one terephthalic acid ligand away from the vanadium center or by removing bridging oxygen between the neighboring vanadium centers from the O–V–O axis. In view of these structural defects in the periodic structure, we opted to simulate the reaction pathways in a cluster model. The numerical algorithms to search for transition states are better established in the computational programs used for the cluster calculations compared with their periodic equivalents. Of course the cluster should be chosen large enough to represent the real active environment within the MIL-47 topology. In view of this, we propose the extended cluster model as displayed in Fig. 8. This model contains two vanadium atoms, bridged by two terephthalate linkers. On the vanadyl chain, only two V=O bonds are maintained, and the continuation to further terephthalate linkers is interrupted and replaced by terminating OH-groups. Starting from this cluster, one can search for the optimized geometry by relaxing all atoms or by fixing the outer carboxyl oxygen atoms at their crystal positions to prevent unphysical deformation of the cluster, while relaxing all other atoms during the geometry optimization. When taking into account dispersion interactions, the constrained geometry is favored by about 42 kJ/mol. Moreover, the obtained result is a realistic representation of the actual molecular environment around the active site in the MIL-47. The MIL-47 (with V^{+IV}) is one of the MOF structures that only shows a small degree of flexibility, and thus, this model should be well suited. Although for completeness, we also performed all calculations in the model in which all atoms are relaxed, allowing as such too much conformational flexibility. In particular, the angle between the two terephthalate planes containing the two terephthalic linkers changes largely during such computational protocol. While this particular angle amounts to

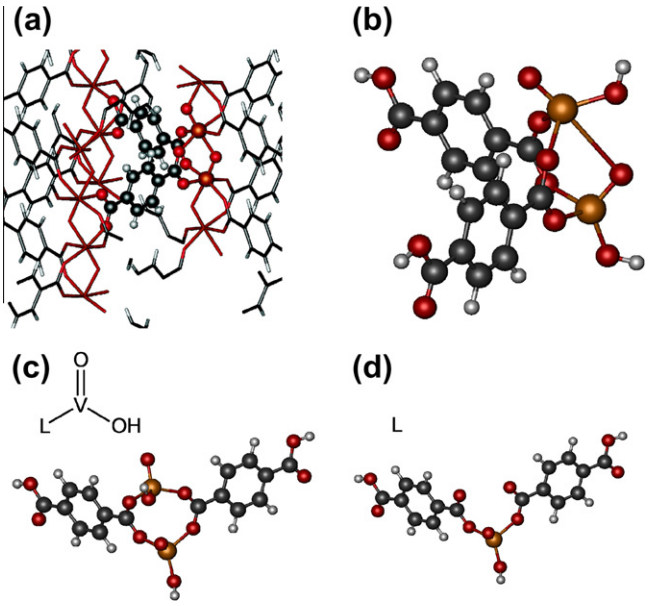

Fig. 8. (a) selected cluster (in balls) in the MIL-47 crystal structure, (b) cluster cut out from the crystal as indicated in (a) is now terminated with hydrogens and is chosen large enough to represent the active site in MIL-47, (c) schematical representation of the extended cluster as displayed in (c), (d) bidentate ligand represented by L. Geometry following the unconstrained model for (c) and (d).

98.5° when the outer atoms are fixed, this angle increases by 12° in the completely unconstrained model. The other geometrical parameters are not substantially different, even the distance between the two V-centers remains almost unaltered for both cluster models (3.80 versus 3.81 Å, compared to 3.42 Å in the MIL-47 crystal). As will be seen later, the deviancy in spatial orientation of the linkers leads to important changes in the kinetics of the reactions with non-negligible impact on the preferential pathways.

The cluster model is schematically shown in Fig. 8c, where L represents a bidentate ligand (Fig. 8d) and hence shows a twofold coordination with V. Notice that the ligand L in the cluster model contains also a V atom, but this site is not regarded as catalytically active during the simulations. The upper vanadium atom as shown in Fig. 8c is taken as the active catalytic center. Both vanadium atoms have oxidation state +IV in the starting cluster model.

3.2.2. Possible reaction pathways toward formation of cyclohexene oxide

The reaction cycle starts with an activation step, in which TBHP coordinates with the vanadium center to form an alkylperoxo species **7** (as shown in Scheme 2). The two most probable reaction routes toward epoxidation starting from this complex are displayed in Scheme 2. First, a direct pathway to epoxidation leads to the formation of cyclohexene oxide **2** and brings the catalyst to a less active complex **8**. Secondly, a radical mechanism is plausible (indicated as "radical" in Scheme 2). In this route, +V vanadium complexes **9** are formed by homolytic cleavage of the peroxy linkage that can then be further activated with TBHP. The generated V^{+V}-activated complexes **10** and **12** can again epoxidize cyclohexene. Both direct and radical routes are completed by a regeneration step that closes the cycle.

Apart from the complexes given in Scheme 2, other possible V^{+V} (OOtBu) complexes can be formed, which also lead to cyclohexene epoxidation. All these plausible pathways have been investigated in this work, but they turned out to be not competitive with respect to those taken up in Scheme 2. We disregard them from further discussion.

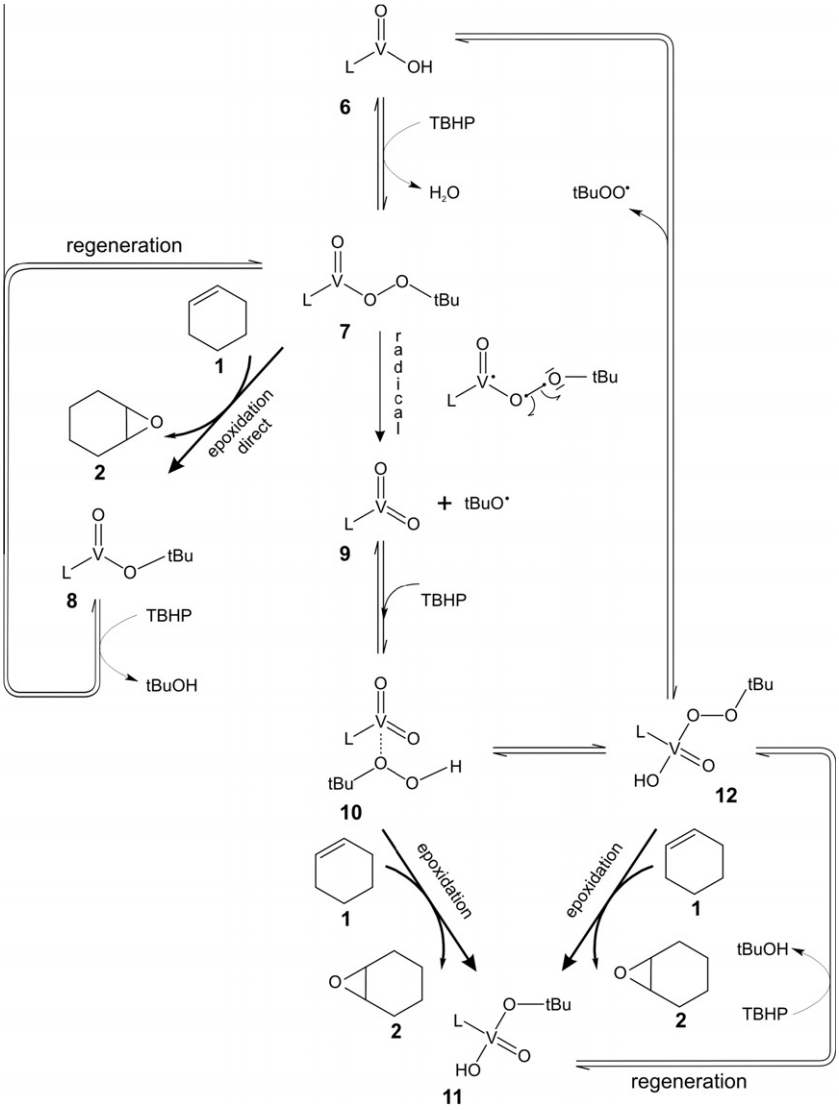

Scheme 2. Two competitive cyclohexene epoxidation pathways for MIL-47 (direct and radical).

3.2.2.1. Reaction kinetics: direct versus radical pathway. For each reaction path energy barriers, Gibbs-free energies at 323 K and reaction rates have been computed in the two models for geometry optimization (unconstrained versus constrained) as outlined before. The results are given in Table 3. All energetics have been calculated within the B3LYP/6-311 + g(3df,2p)-D3//B3LYP/6-31 + g(d) level of theory. The B3LYP/6-311 + g(3df,2p) energies were further refined by including van der Waals interactions at the B3LYP-D3 level of theory with the Orca software package [35]. For the constrained model, we used the partial Hessian vibrational analysis (PHVA) method for the frequency calculations making use of the in-house developed software module TAMkin [36,37]. The outer oxygen atoms, which were used to fix the cluster, were given an infinite mass [38–42]. All structures for starting geometries were built using ZEOBUILDER [37,43].

The kinetics for all epoxidation reactions are obtained using the bimolecular approach in which the two reactants are treated in gas phase. In this case, bimolecular transition state theory should be applied as outlined in Supporting Information. More details are also given by Van Speybroeck et al. [44] on the computational procedures for discriminating between intrinsic and apparent reaction kinetics.

To give an idea on the values of the physisorption energy for the various species, the complete energy diagram is taken up in Fig. 9 for the direct path 7 → 8.

The physisorption energy of cyclohexene is of about −28 kJ/mol, while −70 kJ/mol for the epoxide. However, the position of the cyclohexene/epoxide in the adsorbed complex and the way these molecules are coordinated with the V-center is not always uniquely determined, and therefore, the reaction kinetics is performed starting from the gas-phase species in this study.

The direct epoxidation reaction 7 → 8 is irreversible as can easily be seen from the energy diagram of Fig. 9. Similar large reaction energies are observed for the other epoxidation reactions. Therefore, only the rate constants for the forward reactions are taken up in Table 3. For convenience of the reader, the backward reaction barriers and Gibbs-free energies are also tabulated in Table S1.

The transition state of the direct epoxidation reaction 7 → 8 is given in Fig. 11a. The cyclohexene molecule is located in the free spot that extends to a whole hemisphere in front of the two remaining linkers and the t-butoxy group, stressing once more that the epoxidation reaction can only take place if some ligands are removed.

Table 3
Energy barriers and Gibbs-free energy barriers for the epoxidation reactions (bimolecular) and the radical decomposition (unimolecular). Also the reaction energies are reported, as well the reaction Gibbs-free energies at 323 K.

	Unimolecular			Bimolecular				
	$\Delta E^{\ddagger}_{0,intr}$ (kJ/mol)	$\Delta G^{\ddagger}_{323,intr}$ (kJ/mol)	$k^{unimol}_{323,intr}$ (s^{-1})	$\Delta E^{\ddagger}_{0,app}$ (kJ/mol)	$\Delta G^{\ddagger}_{323,app}$ (kJ/mol)	$k^{bimol}_{323,app}$ ($m^3\ mol^{-1}\ s^{-1}$)	$\Delta E_{0,r}$ (kJ/mol)	$\Delta G_{323,r}$ (kJ/mol)
Unconstrained model								
Direct 7 → 8	–	–	–	−2.8	46.3	5.71E+03	−157.7	−174.8
Radical 7 → 9	37.1	32.9	3.22E+07	–	–	–	28.5	−34.7
10 → 11	–	–	–	35.1	89.6	5.73E−04	−219.4	−213.3
12 → 11	–	–	–	26.8	82.9	6.97E−03	−191.9	−187.2
Constrained model								
Direct 7 → 8	27.4	40.3	2.02E+06	−1.0	48.9	2.19E+03	−157.3	−171.2
Radical 7 → 9	38.0	35.2	1.37E+07	–	–	–	23.8	−37.3
10 → 11	–	–	–	29.1	90.2	4.69E−04	−226.5	−220.3
12 → 11	–	–	–	41.9	107.0	8.87E−07	−189.8	−177.8

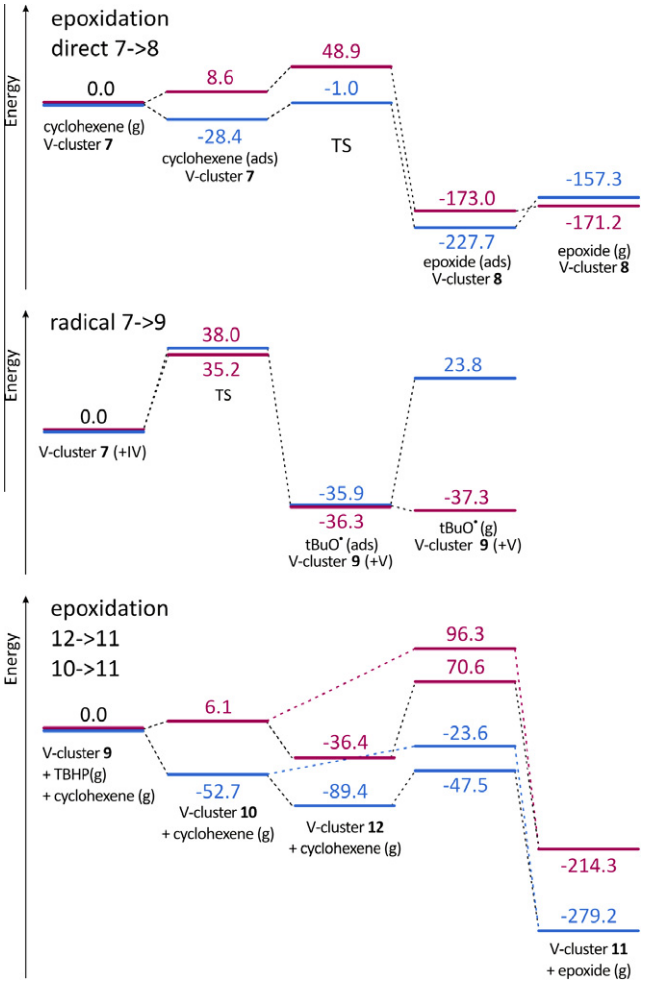

Fig. 9. Energy diagram for the direct epoxidation reaction 7 → 8, the radical reaction pathway 7 → 9 and the subsequent epoxidation reactions 10 → 11 and 12 → 11. Energies (at 0 K) are given in blue, Gibbs-free energies at 323 K are given in red. All energies in kJ/mol. The V-cluster appears as an activated complex in the reactants and as an inactivated complex in the products. In radical reaction 7 → 9 the oxidation number of vanadium changes from +IV to +V. Both energy (at 0 K) and Gibbs-free energy (at 323 K) profiles are drawn relative with respect to the first level in each scheme. Numerical results are obtained using the constrained cluster model. (For interpretation of the references to color in this figure legend, the reader is referred to the web version of this article.)

The constrained and unconstrained models predict nearly the same reaction barriers and entropic contributions (see Table 3) as the geometries resulting from the models only differ in the spatial orientation of the two remaining linkers. The energy diagram of Fig. 9 learns that the reaction is strongly exergonic and thus irreversible.

The direct route **7** → **8** is highly favored on basis of the energy barriers and Gibbs-free energies of activation. The reactions **10** → **11** and **12** → **11** are higher activated (90.2 kJ/mol and 107.0 kJ/mol versus 48.9 kJ/mol for the Gibbs-free energy of activation $\Delta G^{\ddagger}_{323,app}$ following the constrained model Table 3) but are thermodynamically driven as the product **11** is very stable (Gibbs reaction-free energies of −220.3 and −177.8 kJ/mol). The epoxidation reactions **10** → **11** and **12** → **11** are initiated by a radical decomposition **7** → **9** thereby bringing the active V-site into an oxidation state +V followed by a reaction of the originally inactive V-complex **9** with TBHP to an active complex **10** or **12**. The radical decomposition (**7** → **9**) is modeled as an unimolecular process with a reaction barrier of 37–38 kJ/mol or a Gibbs-free energy barrier of 33–35 kJ/mol at 323 K, which thus slightly decreases with temperature. This reaction will certainly take place, and in addition, it is also thermodynamically favored as the reaction becomes more and more exergonic with temperature due to entropic effects (see Fig. 9). Some transformations taken up in Scheme 2 are modeled as equilibration steps and the values are taken up in Table 4. Starting from complex **9**, an equilibration step occurs in which the TBHP coordinates with species **9**, to form another V^{+V} species **10**. This step is thermodynamically controlled toward species **10** at lower temperatures. Species **10** can further transform to species **12**, in which TBHP covalently bonds to the vanadium center. The equilibrium of this step lies in the direction of V-cluster **12**. From species **10** and **12** that are both V^{+V} species, the epoxidation of cyclohexene can be initiated.

Overall, the whole reaction cycle starting from **7** to **11** is very exothermic and also irreversible as the backward reactions have very high activation barriers (up to 300 kJ/mol (see Table S1)). In this "radical" pathway, which allows transformation of oxidation state from +IV to +V for vanadium, one of the epoxidation reactions **10** → **11** and **12** → **11** becomes the rate determining step.

They are higher activated but eventually become also important as this reaction cycle is thermodynamically controlled.

The reaction **12** → **11** requires some special interest as the results are more sensitive to the particular model used for the kinetics calculations, i.e., constrained versus unconstrained. In contrast

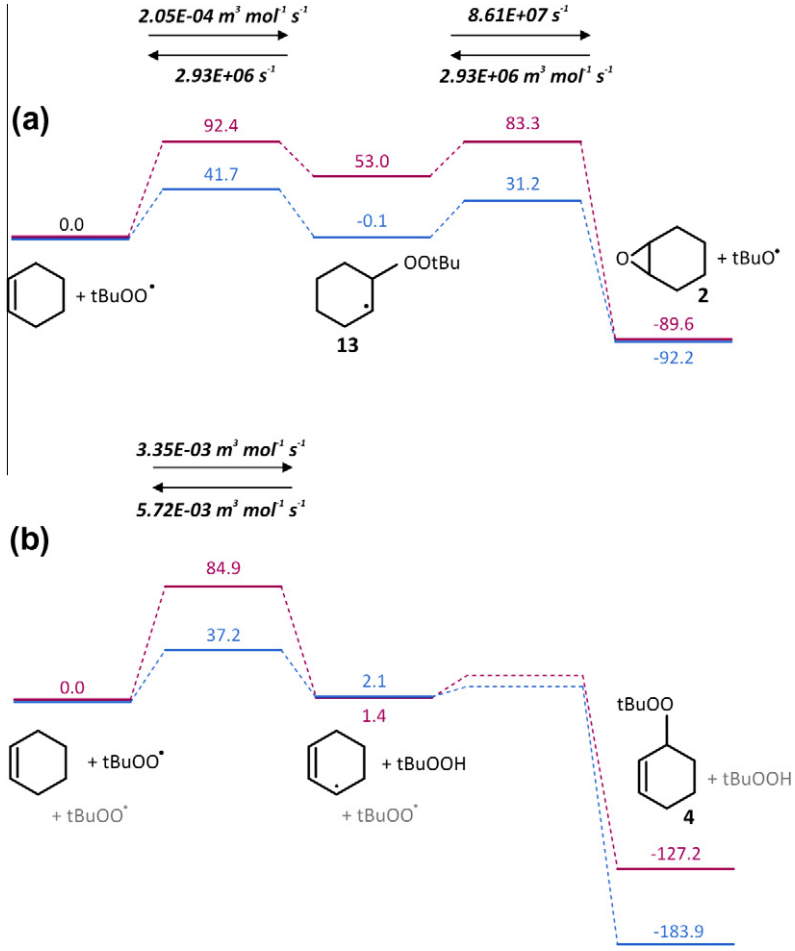

Fig. 10. Energy profiles for the reaction between cyclohexene and the *tert*-butylperoxy radical. Energies (at 0 K) are given in blue, Gibbs-free energies at 323 K are given in red. All energies in kJ/mol. (a) Pathway a leading to formation of cyclohexene oxide. (b) Pathway b leading to formation of the adduct **4**. Electronic energies at 0 K are indicated in red. Energies in kJ/mol. (For interpretation of the references to color in this figure legend, the reader is referred to the web version of this article.)

to the direct pathway **7** → **8** with a V^{+IV} active complex, steric hindrance lies now on the origin of the significant increase of the barrier in the constrained cluster model. In this V^{+V} complex (Fig. 11d), the position of the cyclohexene in the transition state is slightly different with that in the V^{+IV} complex (Fig. 11a). In addition, the free spot for the coordination of cyclohexene is more limited in the V^{+V} complex, and in the constrained model, one of the linkers causes a steric repulsive effect on the cyclohexene, inducing an asymmetric spatial position with respect to the oxygen of the V-complex. This unphysical situation causes too high barriers. Realistically, the values will lie in between the values of the two models and overall the conclusions on the most preferable pathway to epoxidation are not altered. The two geometries of the transition state are visualized in Fig. 11c and d where we can easily see that in the unconstrained case, the position of the linker is more relaxed allowing the cyclohexene to take the most favorable position in the transition state.

The regeneration reactions with TBHP go smoothly as they are mostly thermodynamically driven (see Table 4).

It is now interesting to couple our theoretical results to the available experimental data. The quantitative values of our calculations can indirectly be validated with the results of a kinetic study on the epoxidation of cyclohexene with $VO(acac)_2$. Gould et al. [45] suggested that vanadium is probably converted to the +V oxidation state and remains in that state throughout. This is in full agreement with the situation encountered in the epoxidation reactions **10** → **11** and **12** → **11**. The experiment reports values of 53.1 kJ/mol for the enthalpy of activation and −82.8 J/K/mol for the entropy of activation. For T = 323 K, this results to a Gibbs-free energy of activation of about 80 kJ/mol, which is in excellent agreement with the theoretical predictions for the pathways **10** → **11** and **12** → **11**, which proceed through a vanadium in oxidation state +V.

Summarizing, there are two pathways which are competitive and which form a closed cycle of epoxidation and regeneration and wherein the peroxide is systematically used to bring the inactive vanadium complex (species **6**) into an active complex with oxidation state +IV (species **7**) or an active complex with oxidation state +V (species **10** and **12**). The two epoxidation pathways start from a complex with another oxidation state for vanadium, but a switch from one cycle to the other is possible at any time. Once V^{+V} complexes are formed, a return to the V^{+IV}-cycle is possible via the equilibration step **12** → **6**, which we will call the V^{+V}–V^{+IV} recycling step for further reference. This step is energetically not favored ($\Delta E_{0,r}$ = 132–135 kJ/mol in Table 4) but becomes possible at temperatures of 323 K due to entropic contributions, which bring the free energy of reaction to reasonable values 67–77 kJ/mol. These barriers are of the same order as the barriers for epoxidation and are thus competitive with these pathways.

Thus far, no solvent effects have been taken into account. In the experimental part, the catalytic activity of the MIL-47 has been investigated with TBHP dissolved in water or in decane. One of the main differences was the much larger initiation time for cyclohexene conversion with decane as solvent. The proposed reaction scheme may serve to explain some of the experimental findings. The reaction cycle can only start once free coordination positions are created, either by folding a ligand away or by removing a

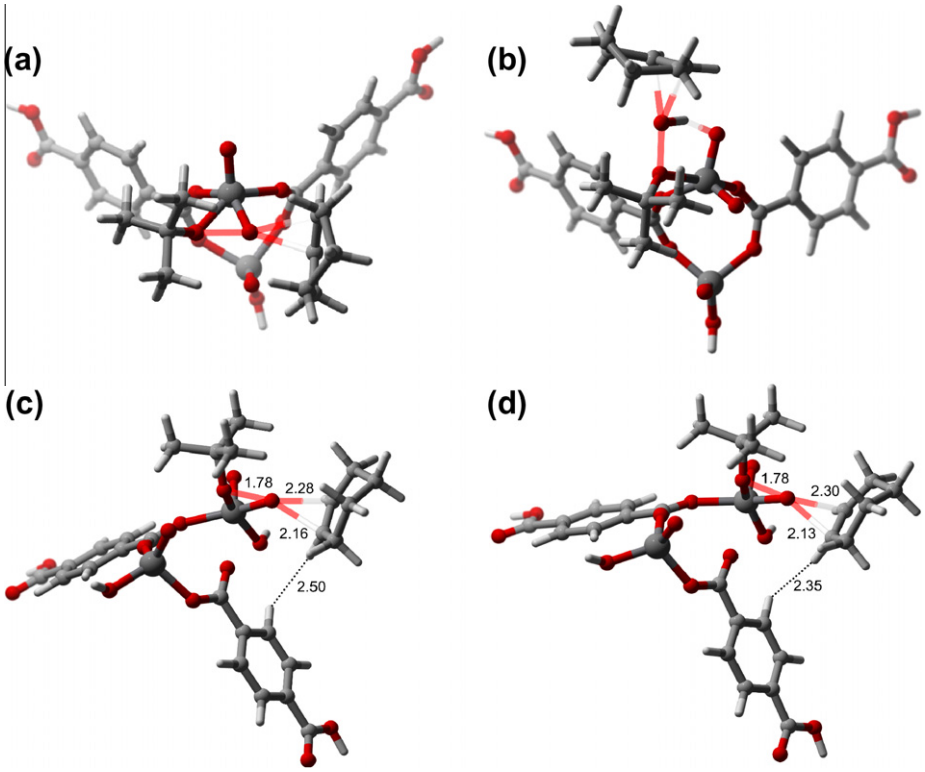

Fig. 11. Transition states of the three epoxidation reactions: (a) direct pathway 7 → 8, (b) pathway 10 → 11, (c) and (d) pathway 12 → 11. Use of the unconstrained model in (a)–(c); use of the constrained model in (d).

Table 4
Thermodynamical parameters for the reactions modeled as equilibrium steps. $\Delta E_{0,r}$ represents the reaction energy corrected with zero-point energies and dispersion, $\Delta G_{323,r}$ the reaction-free energy at 323 K. The equilibrium constant K_{323} at 323 K is obtained after a fitting procedure between 273 and 373 K.

	$\Delta E_{0,r}$ (kJ/mol)	$\Delta G_{323,r}$ (kJ/mol)	K_{323}	$[K_{323}]$
Unconstrained model				
6 → 7	−59.8	−40.8	3.96E+06	–
8 → 7 (regeneration)	−27.5	−7.4	1.55E+01	–
11 → 12 (regeneration)	6.7	5.0	1.53E−01	–
9 → 10	−64.7	−4.8	1.60E−01	$m^3\ mol^{-1}$
10 → 12	−27.5	−26.1	1.67E+04	–
12 → 6 (V^{+V}–V^{+IV} recycling)	132.2	67.6	4.41E−10	m^{-3} mol
Constrained model				
6 → 7	−60.3	−42.3	7.02E+06	–
8 → 7 (regeneration)	−27.9	−10.9	5.73E+01	–
11 → 12 (regeneration)	4.6	−4.3	4.94E+00	–
9 → 10	−52.7	6.1	2.74E−03	$m^3\ mol^{-1}$
10 → 12	−36.7	−42.5	7.54E+06	–
12 → 6 (V^{+V}–V^{+IV} recycling)	134.6	77.2	1.21E−11	m^{-3} mol

terephthalic acid from vanadium. The structure **6** in scheme 2 can be created by cleaving a terephthalate–vanadium bond and replacing the ligand by a hydroxyl group. Such hydroxyl groups can easily be introduced in a water-based medium and thus water helps in creating free coordination sites, enhancing the initial rate of cyclohexene conversion. In case of decane as solvent, such sites of type **6** are not formed as this solvent has no OH-group present. In this case, the activation should be induced by TBHP itself. This can either lead to the cleavage of a vanadium bond and an oxygen of the carboxylate group to form complex **7** immediately but also other species such as VO(L)(OtBu) could be formed, which can by ligand exchange with TBHP form the active species **7**. Therefore, one can anticipate that the initiation time for epoxidation is larger in case of decane, as TBHP takes also an active role in the activation period. These findings are compatible with the observation that the measured experimental diffraction pattern does not change after reaction with TBHP/decane + cyclohexene. The bulk structure remains better conserved during the reaction cycle, whereas in case of water, more vanadium/terephthalic acid bonds are broken. The diffraction pattern of the catalyst with TBHP/water after catalysis (see Fig. 5c) shows a broadening of the peaks that might be ascribed to further structure deterioration.

Another feature observed experimentally is the formation of side products, such as diols, adducts, and cyclohexenones, which are manifestly present after a short reaction time on a MIL-47 catalyst with a V-loading of 0.42 mmol and with TBHP dissolved in water. The experiment with TBHP in decane as oxidant does not reveal any relevant by-product formation. The formation of the *tert*-butyl-2-cyclohexenyl-1-peroxide **4** must be ascribed to radical pathways between the substrate and the oxidant TBHP and was recently further investigated for unsaturated Co-MOFs [14,46]. Freely diffusing peroxy radicals can be generated by a variety of mechanisms in which the oxidation state of vanadium changes. It is well known that radicals are better stabilized in water than in decane and thus such radical pathways are more prominent present in such polarisable media. Also the radicals tBuO• and tBuOO•, appearing in some pathways of Scheme 2, lie on the origin of the formation of the side products, and in particular that of the adduct **4** as schematically shown in Fig. 10 (pathway b). An enhanced concentration of radicals leads to more termination reactions and hence a larger production of adducts. The increasing concentration of the of *tert*-butylperoxy radical tBuOO• requires some attention, as it is also able to directly epoxidize cyclohexene following the so-called Twigg mechanism as reported by Van Sickle et al. [47] (pathway a in Fig. 10). We examine the two competitive pathways. In the first, a radical addition reaction takes place creating an intermediate cyclohexenyl radical **13** followed by cleavage of the

tert-butylperoxy radical and formation of cyclohexene oxide. The energy profile is displayed in Fig. 10 (pathway a). The radical addition reaction shows a high free-energy barrier, while the reaction is strongly endergonic, indicating that the backward reaction (dissociation) goes much faster than the forward reaction (association). In pathway b, a hydrogen abstraction occurs from the allylic position of cyclohexene forming the 3-cyclohexenyl radical, which can rapidly recombine with another *tert*-butylperoxy radical yielding the adduct **4**. The hydrogen abstraction also requires a high energy barrier (only 8 kJ/mol lower than in pathway a). The subsequent radical recombination reaction goes quite quickly since the reaction energy is strongly negative and heavily thermodynamically driven. These theoretical findings are in complete agreement with the suggestions made in a recent experimental work of Tonigold et al. [46] where pathway b has been proposed as the major pathway. Concluding, without excluding the direct epoxidation of cyclohexene by the *tert*-butylperoxy radical tBuOO•, the radical pathway will favor the adduct formation.

4. Conclusions

This study reveals that V-MIL-47 can be a highly selective catalyst in the epoxidation of cyclohexene using TBHP as the oxidant. Water should be avoided as the solvent for the peroxide, as it enhances strongly the leaching of the V-centers and as it accelerates an unwanted radical side reaction, forming an adduct between the peroxide and cyclohexene.

When decane is used to dissolve the peroxide, the MIL-47 is a highly selective catalyst toward the epoxide, especially in the first linear regime of conversion. The leaching of V-centers is negligible in that case and the structural integrity of the MOF is preserved during successive runs. Computational studies show that several catalytic pathways co-exist and compete with each other, but every catalytic cycle starts with the breaking of two V-terephthalic bonds to coordinate with the peroxide. EPR and NMR studies confirm that approximately 20% of the V^{+IV} sites are oxidized to V^{+V} in the first minutes of the catalytic reaction and remain relatively constant afterward.

Acknowledgments

K.L. is grateful to the Long Term Structural Methusalem Grant Nr. 01M00409 Funding by the Flemish Government. M.V. thanks the research board of Ghent University (BOF). I.M. thanks the Institute for the Promotion of Innovation through Science and Technology in Flanders (IWT Vlaanderen). Furthermore, this research is co-funded by the Ghent University, GOA Grant Nr. 01G00710, BELSPO in the frame of IAP 6/27 and the European Research Council (FP7(2007-2013) ERC Grant Nr. 240483). Computational resources (Stevin Supercomputer Infrastructure) and services were provided by Ghent University.

Appendix A. Supplementary material

Supplementary data associated with this article can be found, in the online version, at doi:10.1016/j.jcat.2011.09.014.

References

[1] B.F. Hoskins, R.J. Robson, J. Am. Chem. Soc. 112 (1990) 1546.
[2] H. Li, M. Eddaoudi, M. O'Keeffe, O.M. Yaghi, Nature 402 (1999) 276.
[3] N.L. Rosi, J. Eckert, M. Eddaoudi, D.T. Vodak, J. Kim, M. O'Keeffe, O.M. Yaghi, Science 300 (2003) 1127.
[4] L.J. Murray, M. Dinca, J.R. Long, Chem. Soc. Rev. 38 (2009) 1294.
[5] L. Pan, B. Parker, X.Y. Huang, D.H. Olson, J. Lee, J. Li, J. Am. Chem. Soc. 128 (2006) 4180.
[6] J. Perles, M. Iglesias, M.A. Martin-Luengo, M.A. Monge, C. Ruiz-Valero, N. Snejko, Chem. Mater. 17 (2005) 5837.
[7] D. Farrusseng, S. Aguado, C. Pinel, Angew. Chem. Int. Ed. 48 (2009) 7502.
[8] A. Corma, H. Garcia, F.X.L. Xamena, Chem. Rev. 110 (2010) 4606.
[9] P. Van der Voort, M.G. White, E.F. Vansant, Langmuir 14 (1998) 106.
[10] G. Catana, R.R. Rao, B.M. Weckhuysen, P. Van Der Voort, E. Vansant, R.A. Schoonheydt, J. Phys. Chem. B 102 (1998) 8005.
[11] P. Van Der Voort, M. Baltes, E.F. Vansant, Catal. Today 68 (2001) 119.
[12] A. Henschel, K. Gedrich, R. Kraehnert, S. Kaskel, Chem. Commun. (2008) 4192.
[13] N.V. Maksimchuk, K.A. Kovalenko, S.S. Arzumanov, Y.A. Chesalov, M.S. Melgunov, A.G. Stepanov, V.P. Fedin, O.A. Kholdeeva, Inorg. Chem. 49 (2010) 2920.
[14] M. Tonigold, Y. Lu, B. Bredenkötter, B. Rieger, S. Bahnmüller, J. Hitzbleck, G. Langstein, D. Volkmer, Angew. Chem. Int. Ed. 48 (2009) 7546.
[15] N.V. Maksimchuk, M.N. Timofeeva, M.S. Melgunov, A.N. Shmakov, Y.A. Chesalov, D.N. Dybtsev, V.P. Fedin, O.A. Kholdeeva, J. Catal. 257 (2008) 315.
[16] H. Garcia, A. Dhakshinamoorthy, M. Alvaro, Chem. – A Eur. J. 17 (2011) 6256–6262.
[17] H. Garcia, A. Dhakshinamoorthy, M. Alvaro, Chemcatchem 2 (2010) 1438–1443.
[18] F.X.L.I. Xamena, O. Casanova, R.G. Tailleur, H. Garcia, A. Corma, J. Catal. 255 (2008) 220–227.
[19] J.S. Seo, D. Whang, H. Lee, S.I. Jun, J. Oh, Y.J. Jeon, K. Kim, Nature 404 (2000) 982.
[20] L.Q. Ma, C. Abney, W.B. Lin, Chem. Soc. Rev. 38 (2009) 1248.
[21] C.D. Wu, A. Hu, L. Zhang, W.B. Lin, J. Am. Chem. Soc. 127 (2005) 8940.
[22] L.L. Wen, F. Wang, J. Feng, K.L. Lv, C.G. Wang, D.F. Li, Cryst. Growth Des. 9 (2009) 3581.
[23] P. Phuengphai, S. Youngme, P. Gamez, J. Reedijk, Dalton T. 39 (2010) 7936.
[24] S. Neogi, M.K. Sharma, P.K. Bharadwaj, J. Mol. Catal. A – Chem. 299 (2009) 1.
[25] S. Horike, M. Dinca, K. Tamaki, J.R. Long, J. Am. Chem. Soc. 130 (2008) 5854.
[26] F. Gandara, E.G. Puebla, M. Iglesias, D.M. Proserpio, N. Snejko, M.A. Monge, Chem. Mater. 21 (2009) 655.
[27] J. Juan-Alcaniz, E.V. Ramos Fernandez, U. Lafont, J. Gascon, F. Kapteijn, J. Catal. 269 (2010) 229.
[28] M.J. Ingleson, J.P. Barrio, J.B. Guilbaud, Y.Z. Khimyak, M.J. Rosseinsky, Chem. Commun. (2008) 2680.
[29] A. Dhakshinamoorthy, M. Alvaro, H. Garcia, Catal. Sci. Technol. 1 (2011) 856–867.
[30] K. Leus, I. Muylaert, M. Vandichel, G.B. Marin, M. Waroquier, V. Van Speybroeck, P. Van der Voort, Chem. Commun. 46 (2010) 5085.
[31] K. Barthelet, J. Marrot, D. Riou, G. Ferey, Angew. Chem. Int. Ed. 41 (2001) 281.
[32] A. Brückner, Top Catal. 38 (1–3) (2006) 133.
[33] A. Fenn, M. Wächtler, T. Gutmann, H. Breitzke, A. Buchholz, I. Lippold, W. Plass, G. Buntkowsky, Solid State Nucl. Mag. 36 (2009) 192.
[34] (a) E.P. Talsi, V.D. Chinakov, V.P. Babenko, K.I. Zamaraev, J. Mol. Catal. 81 (1993) 235;
(b) H. Mimoun, M. Mignard, P. Brechot, L. Saussine, J. Am. Chem. Soc. 108 (1986) 3711.
[35] ORCA. 2.6.35ed. <http://www.thch.uni-bonn.de/tc/orca/>.
[36] A. Ghysels, T. Verstraelen, K. Hemelsoet, M. Waroquier, V. Van Speybroeck, J. Chem. Inf. Model. 50 (2010) 1736.
[37] CMM Code. <http://molmod.ugent.be/code/wiki>.
[38] A. Ghysels, D. Van Neck, V. Van Speybroeck, T. Verstraelen, M. Waroquier, J. Chem. Phys. 126 (2007) 224102.
[39] A. Ghysels, D Van Neck, M. Waroquier, J. Chem. Phys. 127 (2007) 164108.
[40] A. Ghysels, V. Van Speybroeck, T. Verstraelen, D. Van Neck, M. Waroquier, J. Chem. Theory Comput. 4 (2008) 614.
[41] A. Ghysels, V. Van Speybroeck, E. Pauwels, D. Van Neck, B.R. Brooks, M. Waroquier, J. Chem. Theory Comput. 5 (2009) 1203.
[42] A. Ghysels, V. Van Speybroeck, E. Pauwels, S. Catak, B.R. Brooks, D. Van Neck, M. Waroquier, J. Comput. Chem. 31 (2010) 994.
[43] T. Verstraelen, V. Van Speybroeck, M. Waroquier, J. Chem. Inf. Model. 48 (2008) 1530.
[44] V. Van Speybroeck, J. Van der Mynsbrugge, M. Vandichel, K. Hemelsoet, D. Lesthaeghe, A. Ghysels, G.B. Marin, M. Waroquier, J. Am. Chem. Soc. 133 (4) (2011) 888.
[45] E.S. Gould, R.R. Hiatt, K.C. Irwin, J. Am. Chem. Soc. 90 (1980) 4573.
[46] M. Tonigold, Y. Lu, A. Mavrandonakis, A. Puls, R. Staudt, J. Mollmer, J. Sauer, D. Volkmer, Chem. Eur. J. 17 (2011) 8671.
[47] D.E. Van Sickle, F.R. Mayo, R.M. Arluck, J. Am. Chem. Soc. 87 (21) (1965) 4824.